INSTITUTE OF PHYSICS PUBLISHING PLASMA PHYSICS AND CONTROLLED FUSION

Plasma Phys. Control. Fusion **45** (2003) 439–453 PII: S0741-3335(03)37221-5

Characterization of turbulence in L- and ELM-free H-mode Wendelstein 7-AS plasmas

N P Basse[1,5,7], S Zoletnik[2,6], G Y Antar[3], J Baldzuhn[4], A Werner[4] and the W7-AS Team

[1] Association EURATOM—Risø National Laboratory, DK-4000 Roskilde, Denmark
[2] CAT-SCIENCE Bt. Detrekő u. 1/b, H-1022 Budapest, Hungary
[3] Fusion Energy Research Program, University of California—San Diego, La Jolla, CA 92093-0417, USA
[4] Association EURATOM—Max-Planck-Institut für Plasmaphysik, D-85748 Garching, Germany

E-mail: basse@psfc.mit.edu

Received 21 May 2002, in final form 5 August 2002
Published 20 March 2003
Online at stacks.iop.org/PPCF/45/439

Abstract

In this paper, measurements of small scale electron density fluctuations in low confinement (L)-mode and high confinement (H)-mode plasmas obtained by collective scattering of infrared light are presented. A single discharge in the Wendelstein 7-AS (W7-AS) stellarator (Renner H *et al* 1989 *Plasma Phys. Control. Fusion* **31** 1579) was studied. The plasma developed from steady-state L-mode to a dithering mode and finally became an edge localized mode (ELM)-free H-mode. These three phases are separately characterized. Autopower spectra of density fluctuations measured in the dithering and ELM-free H-modes are limited to lower frequencies than those in the dithering and steady-state L-modes. Correlations between the density fluctuations, an H_α-signal and magnetic fluctuations as measured by Mirnov coils were analysed. The correlation calculations made for time windows of tens of milliseconds with time lag steps of 100 μs show that all the fluctuating quantities are highly correlated during the L-mode and dithering states, but that no correlation exists in the ELM-free H-mode. Evaluating correlations on a 20 μs timescale between magnetic and density fluctuations leads to the result that the minimum correlation timescale in steady-state and dithering L-modes is of order 100 μs, while no correlation exists for ELM-free and dithering H-modes. Finally, the time derivative of the phase of the measured complex density fluctuation signal allows us to study the structure of turbulent bursts in L- and H-mode.

[5] Also at: Ørsted Laboratory, Niels Bohr Institute for Astronomy, Physics and Geophysics, DK-2100 Copenhagen, Denmark.
[6] Also at: Association EURATOM—KFKI-RMKI, H-1125 Budapest, Hungary.
[7] Present address: MIT Plasma Science and Fusion Center, Cambridge, Massachusetts, USA.

1. Introduction

The study of turbulence during edge and internal transport barrier formation remains an important subject in fusion plasma physics. For an overview of the results so far, we refer to the recent reviews focusing on theoretical [1] and experimental [2] work. In this paper, we will analyse measurements of density fluctuations in a plasma undergoing a transition from the low confinement (L)-mode, through a dithering state and finally entering an edge localized mode (ELM)-free high confinement (H)-mode (also known as the H*-mode [3]). In the dithering phase, the plasma switches quickly between L- and H-mode [4]. The H-mode is characterized by the existence of an edge transport barrier (ETB) in the vicinity of the last closed flux surface (LCFS).

The analysis presented in this paper is an extension of the investigation of dithering plasmas published in [5]. There, we found that density fluctuations in dithering plasmas had distinct properties in the L- and H-mode phases. The remaining question is whether this behaviour is comparable to that of steady-state L-mode and the H*-mode.

To answer this question we analyse density fluctuations in shot 47 114, which was performed on the same day as the series treated in [5]. This discharge developed from L-mode, through a dithering phase and finally made the transition to the H*-mode. We will here compare fluctuations in these three confinement states.

It is at this point pertinent to remark that the analysis was carried out using a single discharge; a larger number of closely matched shots such as those treated in [5] was not available. Another discharge entering H*-mode has been examined in [6], and several other plasma types have been scrutinized in, e.g. [7, 8].

The paper is organized as follows: in section 2, we describe the discharge analysed and the main properties of the localized turbulence scattering (LOTUS) diagnostic. Thereafter, we very briefly describe salient features of the auxiliary diagnostics used in the paper. Autopower spectra of the density fluctuations are studied in section 3; steady-state and dithering phases are compared. Section 4 contains the results of a correlation analysis between H_α-light, magnetic and density fluctuations. Separation of single events using the time derivative of the phase of the complex signal from LOTUS is made in section 5. Finally, the main conclusions are stated in section 6.

2. Overview

2.1. Discharge description

The discharge was separatrix limited with an edge rotational transform ι_a of 0.56 (the '5/9 boundary island' configuration, where the main plasma is bounded by nine magnetic islands [9]) and had a duration of 600 ms. The deuterium plasma was heated by 1 MW hydrogen neutral beam injection (NBI), where the absorbed power is about 75%. The effective plasma minor radius a was 15 cm, with a toroidal magnetic field B_φ of 2.5 T and zero net current. The line density was ramped up throughout the shot (see figure 1). Since the plasma density has to exceed a certain threshold density for the H*-mode to exist [3], the density ramp lead to a L-mode (100–400 ms) $\rightarrow$ dithering H-mode (400–550 ms) $\rightarrow$ H*-mode (550–600 ms) sequence. The improved confinement leads to impurity accumulation, causing a radiation collapse [10] at 600 ms.

Figure 1 shows waveforms of a few of the most important quantities; from top to bottom: stored energy W_{dia} (note the disturbance in the signal from 400 to 550 ms, the dithering phase), line density (ramped up), H_α-light (marking the confinement progression), radial electric

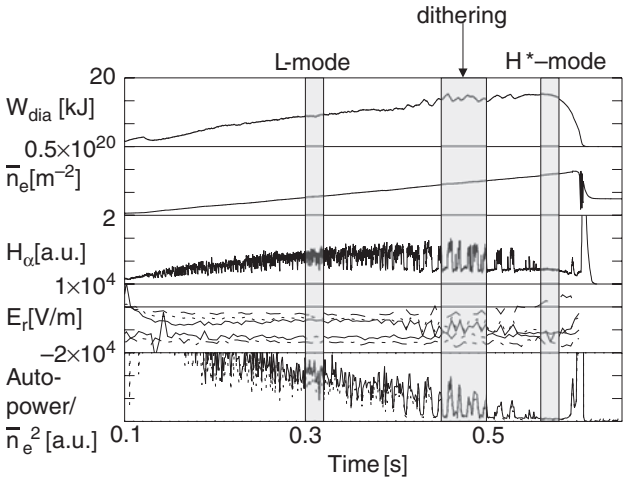

Figure 1. Discharge overview—time traces from 100 to 650 ms. From top to bottom: diamagnetic energy (kJ), line density, H_α-light, radial electric field and frequency integrated density fluctuations (1 ms time windows) in volumes 1 (——) and 2 (· · · · · ·) at $k_\perp = 14\,\mathrm{cm}^{-1}$ normalized by line density squared. The radial electric field is shown for five radial positions: innermost to outermost position is represented by —— (minor radius $r \sim 9$ cm), · · · · · · (10 cm), - - - - (11 cm), — · — (13 cm) and –· · –– (14 cm) lines. The three analysis time windows are marked by grey semi-transparent rectangles.

field E_r at five positions (two inner traces, solid and dotted, clearly displaying the dithering) and density fluctuations normalized by line density squared.

The slow rollover of W_dia during the H*-mode is due to a gradual decrease of the edge temperature gradient [3].

The E_r values are inferred from passive spectroscopic measurements of Boron IV as explained in [11]. According to the lowest order force balance equation, the radial electric field is determined by the poloidal and toroidal velocities and magnetic fields in conjunction with the pressure gradient. In W7-AS, the main component of E_r is normally due to poloidal rotation [11].

We measured the density fluctuations having $k_\perp = 14\,\mathrm{cm}^{-1}$ (or a wavelength of 4.5 mm). The existence of a radial electric field means that the poloidal $\boldsymbol{E} \times \boldsymbol{B}$ frequency is given by the following equation:

$$\omega_{E\times B} = 2\pi \nu_{E\times B} = k_\theta \frac{E_\mathrm{r}}{B_\varphi}, \tag{1}$$

where we use $k_\theta \sim k_\perp$ [12]. A negative (positive) E_r means flow in the electron (ion) diamagnetic drift (d.d.) direction, respectively. Therefore, the switching of E_r somewhat inside the LCFS at about $-10^4\,\mathrm{V\,m}^{-1}$ corresponds to an $\boldsymbol{E} \times \boldsymbol{B}$ frequency of about 900 kHz. We have previously established that $\boldsymbol{E} \times \boldsymbol{B}$ rotation and not drift wave modes are responsible for the major part of the observed frequency shift [5].

Unfortunately, a causal connection between E_r and the density fluctuations can not be established due to the limited time resolution of E_r in this discharge (4 ms). Furthermore, detailed comparisons between turbulence effects and theoretical projections for stabilization of instabilities due to shear in E_r [13, 14] were not possible, mainly due to the low temporal and spatial resolution of the radial electric field measurements and the absence of turbulence codes tailored to W7-AS conditions.

The development of the density fluctuation power closely reflects the confinement behaviour: normalizing by line density squared to obtain a quantity roughly describing the relative fluctuation level, we note that density fluctuations are significantly reduced in entering the H*-mode. The three analysis time windows that will be treated in the following sections are indicated by grey rectangles in figure 1.

2.2. The LOTUS diagnostic

The LOTUS density fluctuation diagnostic has been described in detail elsewhere [15]. We will therefore limit ourselves to a rudimentary description below.

The left-hand side of figure 2 shows a sketch of the diagnostic. The radiation source is a continual wave CO_2 laser yielding 20 W; it is represented by a thick line and denoted the main (M) beam. A small part of the radiation is separated from the M beam and frequency shifted by 40 MHz. This second beam is symbolized by a thin line and called the local oscillator (LO) beam. Both beams are split into two and propagated to the plasma, where two pairs of crossed M and LO beams interfere to form the measurement volumes. The measured wavenumber $k_\perp$ is the same in each volume and proportional to the scattering angle θ_s between the M and LO beams. In the experiments analysed herein the direction of $k_\perp$ was set along the major radius R of the stellarator. It is well-known that the amplitude of density fluctuations peaks for wavenumbers close to $1\,\mathrm{cm}^{-1}$ and decreases rapidly for larger wavenumbers [16]. However, due to limitations in the optical set-up we measured at $k_\perp = 14\,\mathrm{cm}^{-1}$ (the range of wavenumbers accessible with LOTUS lies between 14 and $62\,\mathrm{cm}^{-1}$). Although turbulence is only characterized at one wavenumber, we are of the opinion that the results at larger wavenumbers are well-known, since fluctuations in dithering L- and H-modes at eight different wavenumbers have been treated in [5].

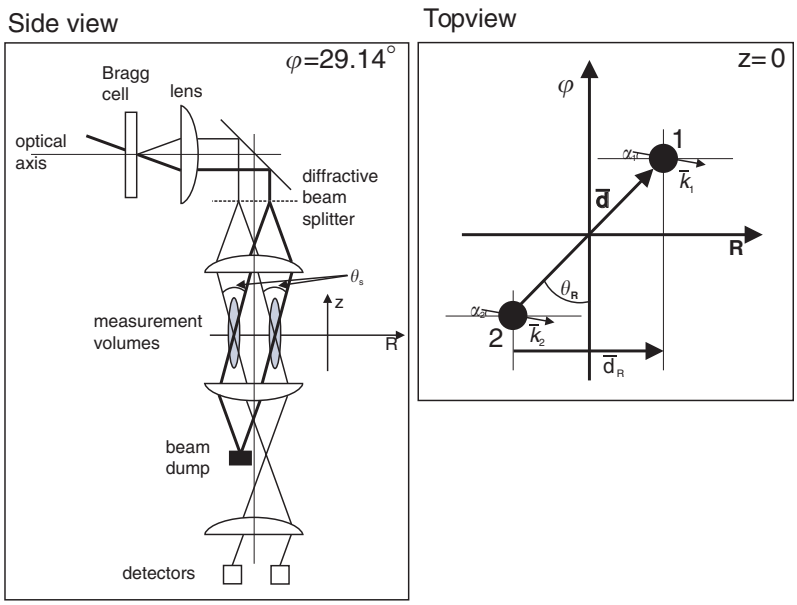

Figure 2. Left: schematic representation of the dual volume set-up (side view). Thick lines are the M beams, thin lines the LO beams, right: the dual volume set-up seen from above. The black dots are the measurement volumes.

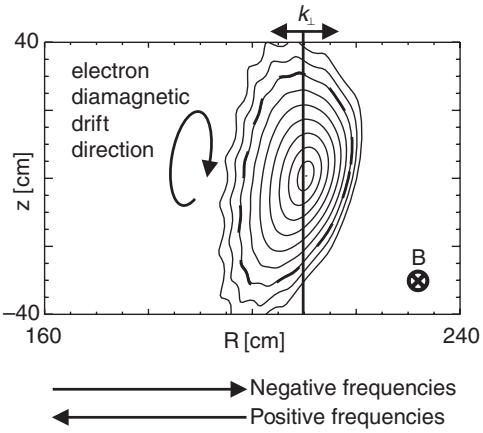

Figure 3. Schematic drawing of the diagnostic set-up on flux surfaces from a shot having a rotational transform of $\frac{1}{3}$ (The W7-AS equilibrium code TRANS could not calculate flux surfaces for the actual transform of $\frac{5}{9}$). The dashed line shows the LCFS due to limiter action. The magnetic field direction and the corresponding electron d.d. direction is indicated. The measured wavenumber is along the major radius R.

The two narrow (diameter $2w = 8$ mm, where w is the beam waist) vertical measurement volumes are shown viewed from the top on the right-hand side of figure 2. The measurement volumes are separated by a distance $d = 29$ mm; the angle θ_R was set to 0°, meaning that the volumes were toroidally displaced. The angles α_1 and α_2 were also set to 0°.

Aligning θ_R so that $\boldsymbol{d}$ (the vector connecting the two measurement volumes) is parallel to the local magnetic field at the top or bottom of the plasma, some spatial localization can be obtained (see, e.g. [7]). However, for the discharge analysed, θ_R was such that $\boldsymbol{d}$ was nearly parallel to the magnetic field in the central plasma. This meant that no spatial information could be extracted. Consequently, measurements in this paper are line integrals of density fluctuations along the volumes through the entire plasma column.

The vertical line in figure 3 indicates the position of the measurement volumes with respect to the flux surfaces. Note that for the actual ι_a of 0.56, the main set of nested flux surfaces is smaller, and that this set is surrounded by nine 'natural' magnetic islands (see, e.g. figure 1 in [9]). The crossing M and LO beams forming the measurement volumes are frequency shifted. Therefore, heterodyne detection is performed, meaning that we can distinguish the direction of the fluctuations as being due to inward (outward) (positive (negative) frequencies) travelling fluctuations parallel to R.

2.3. Complementary diagnostics

The two diagnostics we use for direct comparisons to the density fluctuations are H_α-light signals and magnetic fluctuations measured by Mirnov coils. Since we have already described these standard diagnostics in [5], we offer extremely brief descriptions.

The H_α-emission was measured at an inner limiter; it was sampled at 10 kHz. Magnetic fluctuations in the poloidal field, B_θ, were sampled at 250 kHz using a monitor coil ('MIRTIM'). The behaviour of the magnetic fluctuations is shown in figure 4. The fluctuations in the dithering period (400–550 ms) exhibit a clear burst-like behaviour. We must caution that the spectrogram frequencies may be misleading due to aliasing effects.

3. Autopower spectra

3.1. Spectral analysis tools

The real signals acquired from each detector are centred at the heterodyne carrier frequency of 40 MHz. These are quadrature demodulated to obtain complex signals centred at zero frequency. The resulting signals are denoted

$$S_j(t) = X_j(t) + \mathrm{i}Y_j(t) = A_j(t) \times \mathrm{e}^{\mathrm{i}\Phi_j(t)}, \tag{2}$$

where j is the volume number (1 or 2). We can proceed and calculate

$$P_j(\nu) = \left| \int_{t_1}^{t_2} S_j(t) \mathrm{e}^{-\mathrm{i}2\pi\nu t}\, \mathrm{d}t \right|^2, \tag{3}$$

the autopower spectrum of volume j for a time interval $\Delta t = t_2 - t_1$. The autopower in a certain frequency band $\Delta\nu = \nu_2 - \nu_1$

$$P_j^b = \int_{\nu_1}^{\nu_2} P_j(\nu)\, \mathrm{d}\nu \tag{4}$$

is called the band autopower, as indicated by the lowercase superscript, b, in equation (4).

Finally, the power of the density fluctuations integrated over all frequencies where turbulence is observed is given by

$$P_j = \int_{-\nu_2}^{-\nu_1} P_j(\nu)\, \mathrm{d}\nu + \int_{\nu_1}^{\nu_2} P_j(\nu)\, \mathrm{d}\nu. \tag{5}$$

Note that the frequency interval $[-\nu_1, \nu_1]$ is excluded from the integrals; this is because the signal is dominated by the carrier frequency at low frequencies. In the following (and in figure 1) we use $\nu_1 = 50$ kHz.

3.2. Steady-state and dithering autopower spectra

We begin our description of the density fluctuation autopower spectra by showing a spectrogram of shot 47 114 (volume 1) in figure 5. Density fluctuations are shown up to ± 2 MHz on a logarithmic colourscale; again, the confinement transition sequence is readily observable. ELM or dithering activity manifests itself as high frequency activity, while only low frequency fluctuations remain in H*-mode (after 550 ms). Shortly after entering the H*-mode, a gradually chirping frequency mode develops spinning down as the radiation collapse is approached. It is not clear if these two phenomena are connected.

In figure 6, we compare autopower spectra in the three analysis time windows. The left hand plot shows spectra in the dithering phase separated using the H_α-signal. Basically, a series of L- and H-mode sub-windows are constructed from the H_α-signal by selecting a threshold value of the amplitude. For intervals where the signal is below (above) this threshold, the time window is interpreted as a H- (L-)mode state. The technique is illustrated in [5] (figure 7). The solid line spectrum is L-mode, the dotted line H-mode. The L-mode spectrum extends to higher frequencies than the H-mode spectrum. For positive L-mode frequencies two features seem to be present, above and below 500 kHz.

The right hand plot shows spectra from steady-state L-mode (solid line) and H*-mode (dotted line). The L-mode spectrum is very similar to that during the dithering phase, while the H*-mode spectrum has an additional low amplitude feature at high frequencies; this is the chirping feature mentioned in connection with figure 5. If the chirping feature travels in the electron d.d. direction—as is usually the case for high frequency fluctuations [7]—the feature at 2 (-1) MHz is located towards the bottom (top) of the plasma. The difference in the

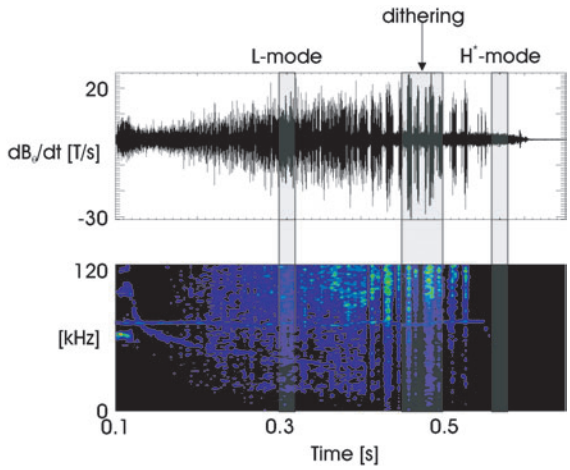

Figure 4. (Colour) Magnetic field derivative in T/s from the MIRTIM monitor coil (top) and a spectrogram (bottom) covering 550 ms. The three analysis time windows are marked by grey semi-transparent rectangles.

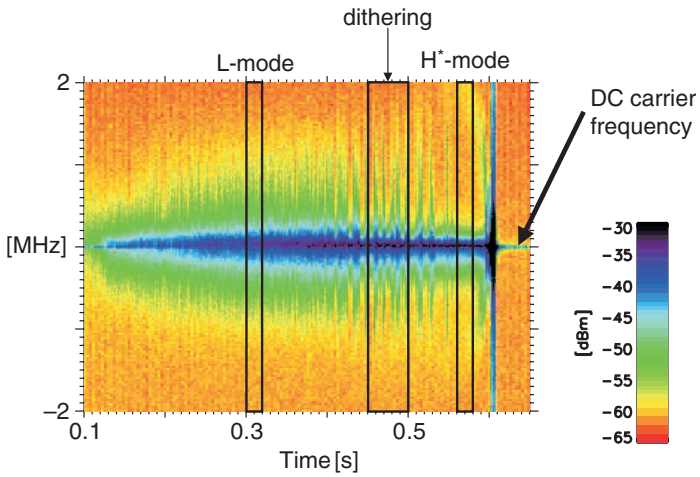

Figure 5. (Colour) Autopower versus time and frequency for discharge 47 114, volume 1. The time resolution of the spectra is 1 ms and the colourscale is logarithmic.

magnitude of the frequency between the top and bottom can be attributed to flux compression effects: since the flux surfaces are more densely spaced at the bottom than at the top of the plasma (roughly by a factor of 2, see figure 3), the flow velocity at the bottom should increase by the same amount to keep the flux constant in a volume element [7]. It is interesting to note that what we here call chirping (spin-down of a feature) is associated with a deteriorating confinement quality in a different type of transitions, created by modifying the rotational transform profile [7].

In [5], we found that the autopower spectra obey a

$$P(k_\perp, \nu) = c_1(k_\perp) \times \mathrm{e}^{c_2(k_\perp)\nu} \tag{6}$$

type scaling [17]. For a given $k_\perp$, c_2 is a direct measure of the slope of the autopower spectra. Fitting the L- and H-mode spectra, it was observed that if one stretches the H-mode frequency

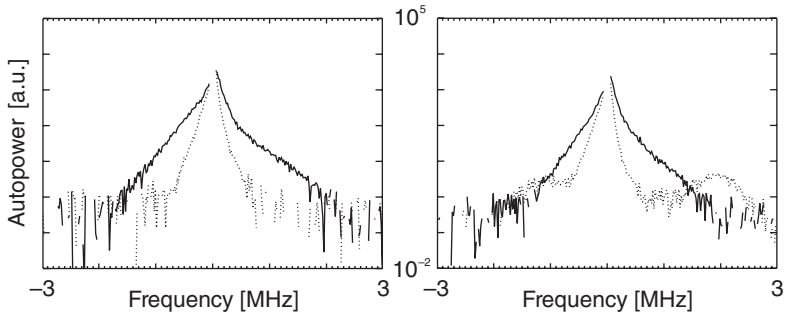

Figure 6. Autopower spectra. Left: L-mode part of dithering phase (——) and H-mode part of dithering phase (· · · · · ·). Right: steady-state L-mode (——) and H*-mode (· · · · · ·).

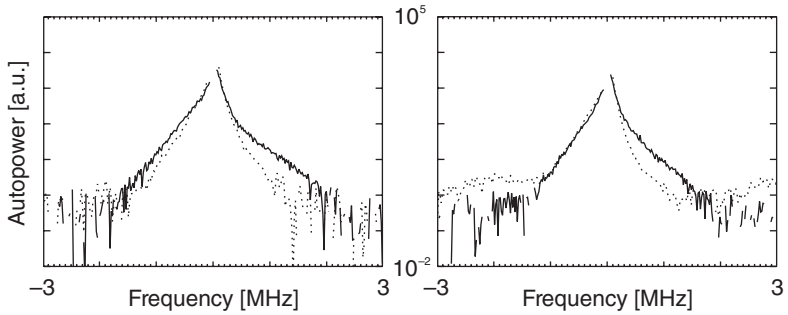

Figure 7. Autopower spectra. Left: L-mode part of dithering phase (——) and H-mode part of dithering phase (· · · · · ·). Right: steady-state L-mode (——) and H*-mode (· · · · · ·). *Note*: The H- and H*-mode frequencies have been scaled by a factor 1.8 (see text).

scale by 1.8 ± 0.3, the H-mode autopower spectrum becomes comparable to the L-mode spectrum.

In figure 7, we show the same L-mode autopower spectra as in figure 6 along with H-mode spectra where the frequencies have been scaled by the factor 1.8 mentioned above. Scaling of the dithering H-mode frequencies brings the low frequency spectra into approximate agreement (for positive and negative frequencies), but cannot account for the high frequency component. Similarly, scaling accounts for the low frequency changes of both signs in the quiescent states.

Maintaining the assumption that $\boldsymbol{E} \times \boldsymbol{B}$ rotation dominates the spectra, the concordance between the L-mode and scaled H-mode spectra means that $|E_\mathrm{r}|$ must be largest in L-mode. However, when we compare L- and H*-mode E_r edge profiles (figure 8), we observe a strong increase in $|E_\mathrm{r}|$ from L- to H*-mode at the two innermost measurement points. The only probable spatial position for the origin of the density fluctuations is the central point ($z = 22\,\mathrm{cm}$); however, E_r is known to become small in the very plasma core as well, where no measurements were available for the discharge. Note that the sign of the central E_r point changes from negative to positive in going from L- to H*-mode. If the density fluctuation frequencies observed were purely due to $\boldsymbol{E} \times \boldsymbol{B}$ rotation, this would indicate a flow reversal from the electron to the ion d.d. direction at the transition from L- to H*-mode. Such a flow reversal is not seen in our measurements; the explanation is that the observed frequency shift is not exclusively due to $\boldsymbol{E} \times \boldsymbol{B}$ rotation, but also has a contribution from drift wave instabilities [5]. In the present case, the most probable instability is the electron drift wave mode, which rotates

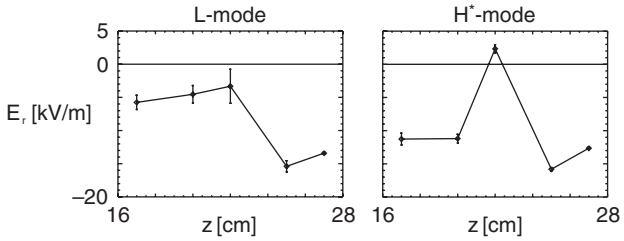

Figure 8. Edge radial electric field E_r as determined by Boron IV spectroscopy versus z. The diagnostic coordinate z is roughly double the minor radius value. Left: L-mode, right: H*-mode.

in the electron d.d. direction. These two components of the frequency shift imply that the net direction of rotation is the electron d.d. direction both in L- and H*-mode.

4. Correlations

In this section on correlations, we correlate density fluctuations, H_α-light and the root-mean-square (RMS) Mirnov coil signal. The measurements which we analyse for possible correlations were not sampled using a common clock (the different analog to digital converters, ADCs, were not synchronized), therefore we will not analyse crosspower spectra. First, we compare dithering to steady-state L- and H*-mode on a 100 μs timescale (section 4.1), thereafter we compare magnetic and density fluctuations on a 20 μs timescale (section 4.2).

The cross covariance between two time series x and y is given as

$$\begin{aligned} R_{xy}(\tau) &= \frac{1}{N}\sum_{k=0}^{N-\tau-1}(x_{k+|\tau|}-\bar{x})(y_k-\bar{y}) \qquad \text{for } \tau < 0, \\ R_{xy}(\tau) &= \frac{1}{N}\sum_{k=0}^{N-\tau-1}(x_k-\bar{x})(y_{k+\tau}-\bar{y}) \qquad \text{for } \tau \geqslant 0, \end{aligned} \tag{7}$$

where τ is time lag and N is the size of the two series [18]. Similarly, the cross correlation is conventionally defined in terms of cross covariances as

$$C_{xy}(\tau) = \frac{R_{xy}(\tau)}{\sqrt{R_{xx}(0) \times R_{yy}(0)}}. \tag{8}$$

For fast (20 μs) cross correlations calculated during the dithering time window we will use a modified version of the function introduced above, $C_{xy}^{\mathrm{mod}}(\tau)$, designed to treat a series of time windows in order to calculate separate L- and H-mode correlations (see [5] for details).

The cross correlations in all the remaining time windows are calculated using the standard definition presented in equation (8).

We will let the band autopower of the density fluctuations be the x series, and y be either the H_α-signal or the power of the Mirnov signal. This means that for positive lags, density fluctuations occur first, while for negative lags, they are delayed with respect to the other series. We will denote the lag where the correlation has a maximum the 'toplag', τ_0 [19]. The cross correlation will be calculated for several density fluctuation frequency bands and represented in contour plots; in these plots we define a global maximum correlation position in (τ, ν)-space: $\tau_0^{\max} = \mathrm{MAX}(\tau_0)^b$.

4.1. Correlated changes in density fluctuations, limiter H_α-emission and magnetic fluctuation power

The comparison between dithering, steady-state L-mode and H*-mode on a 100 μs timescale is summarized in figure 9. The figure shows six contour plots, where the density fluctuation band autopower is correlated with H_α-light and the RMS Mirnov signal. The top row shows correlations for the dithering time interval ([450, 500] ms, see figure 1), centre row for steady-state L-mode ([300, 320] ms) and bottom row for H*-mode ([560, 580] ms).

We emphasize that the frequency scale in figures 9 and 11 refers to density fluctuation frequencies.

Let us begin by studying the top row. It is clear that there is a significant correlation of both the H_α-light and the magnetic fluctuations with the density fluctuations. This implies that the switching of these quantities during dithering is closely connected. The maximum H_α correlation is at zero time lag and largest for the smallest frequency, 150 kHz (about 80%). For low frequencies, a measurable correlation exists beyond 1 ms. At higher frequencies, the long time correlation becomes reduced. The asymmetry for positive lags in the cross correlation is due to the slow decay of the H_α-signal compared to density fluctuations at the L–H transition. The cross correlation with the RMS Mirnov signal is similar to the H_α correlation, but is symmetric around a lag slightly shifted in the negative direction. This means that the density fluctuations are delayed with respect to the magnetic fluctuations. The delay reflects a causal relationship: we have correlated the density fluctuation measurements with several additional

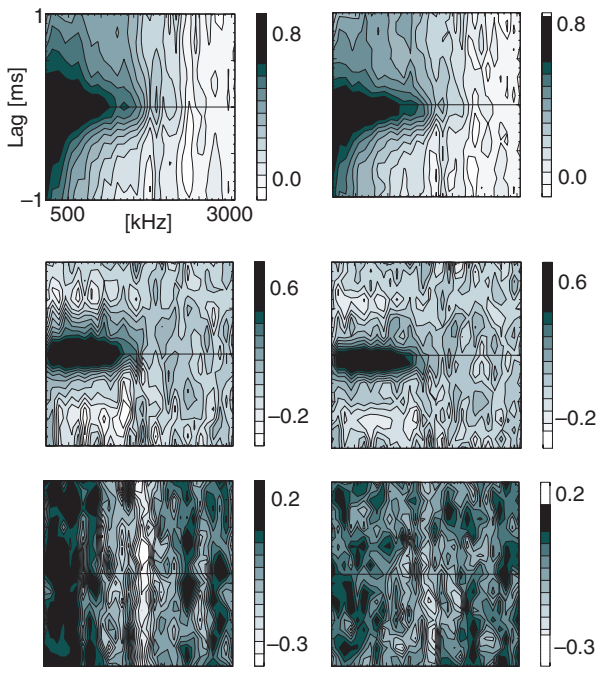

Figure 9. Left column: cross correlation between H_α and density fluctuation band autopower from collective scattering versus band central frequency and time lag (units of 100 μs). Right column: cross correlation between RMS Mirnov signal and density fluctuation band autopower from collective scattering versus band central frequency and time lag (units of 100 μs). Rows from top to bottom: dithering ([450, 500] ms), L-mode ([300, 320] ms) and H*-mode ([560, 580] ms). Note that the greyscale is different for each contour plot.

Mirnov coils at different toroidal and poloidal positions. No evidence of, e.g. rotation induced differences in the time lag has been discovered, so we can conclude that the delay found is indeed an actual time delay.

The correlations in the centre and bottom rows of figure 9 are for steady-state time windows. Correlations in these phases would indicate that turbulent bursts between the fluctuating quantities are coupled.

The centre row shows cross correlations for the steady-state L-mode time window. In this case, the correlation extends only up to a few hundred microseconds and up to 1.5 MHz. Again, the correlation with magnetic fluctuations shows that the density fluctuations are delayed. For both cases the maximum correlation is slightly above 60% and has shifted to about 650 kHz.

Finally, the bottom row shows cross correlations for H*-mode. As is clear, no correlations exist, although density fluctuations remain at a significant level below 500 kHz. The correlation level is between $\pm 20\%$, with no systematic behaviour.

4.2. Correlation between δn_e and $\partial_t B_\theta$ bursts

Above, we correlated fluctuations on a 100 μs timescale; we now turn to the fast (20 μs) cross correlation between magnetic and density fluctuations.

The top row of figure 10 is an analysis of the cross correlation in the dithering phase, where the time windows have been separated using the H_α-signal. The top row shows cross

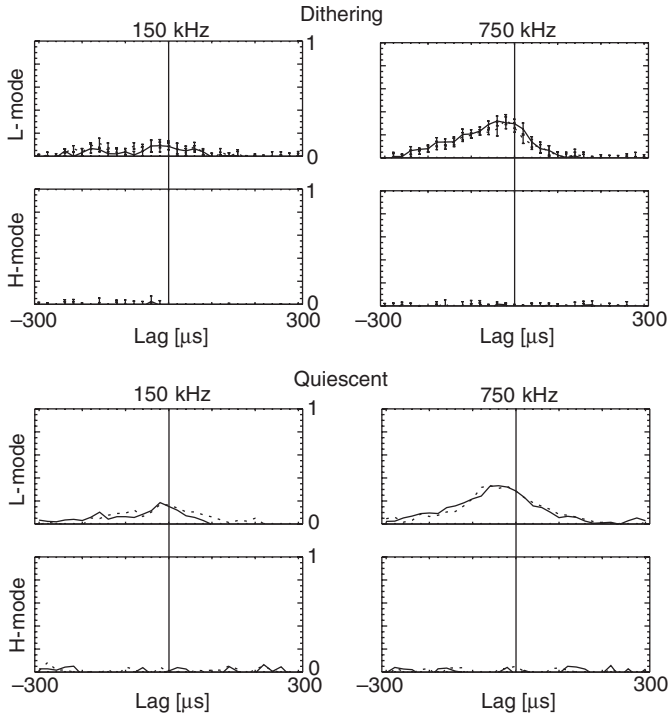

Figure 10. Cross correlation between magnetic and density fluctuations for L- and H-mode time windows versus time lag (units of 20 μs). Top left: cross correlation for 150 kHz dithering density fluctuations, top right: cross correlation for 750 kHz dithering density fluctuations. Bottom left: cross correlation for 150 kHz steady-state density fluctuations, bottom right: cross correlation for 750 kHz steady-state density fluctuations. Solid line is volume 1, dotted line volume 2.

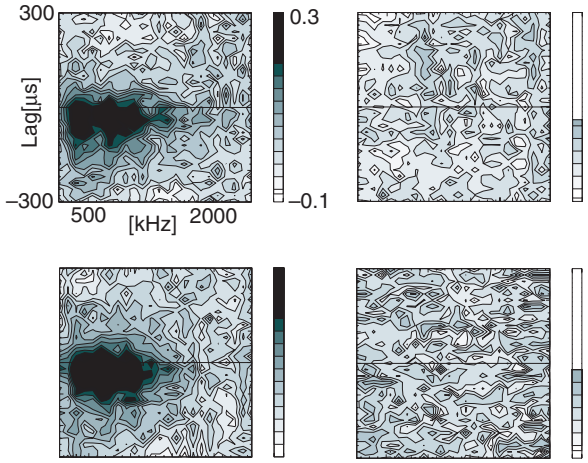

Figure 11. Cross correlation between Mirnov RMS signal and density fluctuation band autopower from collective scattering versus band central frequency and time lag (units of 20 μs). Top left: dithering L-mode, top right: dithering H-mode. Bottom left: steady-state L-mode, bottom right: H*-mode. The greyscale on the right-hand sides of the plots shows what range of the total scale is relevant for the particular time window.

correlations between magnetic and density fluctuations for two frequencies, 150 kHz (left hand plot) and 750 kHz (right hand plot). The top subplots show L-mode results, bottom H-mode. The L-mode fluctuations are weakly correlated at low frequencies, but the H-mode fluctuations are not correlated. At higher frequencies, L-mode fluctuations are clearly correlated. However, H-mode fluctuations remain uncorrelated. The L-mode high frequency toplag is slightly shifted towards negative lags, indicating that the magnetic fluctuations occur about 50 μs before the density fluctuations. The full-width at half-maximum (FWHM) of the correlation is of order 100 μs. The cross correlation in L-mode for high frequencies is seen to be just below 40%.

The bottom row of figure 10 shows the analysis results for steady-state L-mode and H*-mode, also at 150 and 750 kHz. There are no errorbars on these plots since the cross correlation is constructed from only one time interval. It is clear that the cross correlation found in the steady-state phases is almost identical to that found for the dithering plasma.

We have seen that the two-dimensional slices of the cross correlation are close to identical for dithering L- and H-modes and steady-state modes. To verify this for all frequencies, we show contour plots of the cross correlation in figure 11. The top row shows the result for dithering states, left hand L-mode and right hand H-mode. As for the slow time resolution results, a large correlation exists for the dithering L-mode. The time delay is clearly shifted towards negative lags, meaning that the density fluctuations occur after the magnetic fluctuations. No systematic correlation is visible for the dithering H-mode.

The steady-state analysis (bottom row of figure 11) is completely analogous to the results from separating the dithering phase into L- and H-mode. A strong steady-state L-mode correlation up to density fluctuation frequencies of 1.5 MHz and no detectable H*-mode correlation.

5. Phase separation

It would be interesting to inspect the raw density fluctuation signal itself to see if one can tell directly whether a given time interval is L- or H-mode. An ideal tool for this type of study is the derivative of the detected phase (Φ, see equation (2)) with respect to time [20].

The findings reported here represent the first application of the phase derivative technique on different plasma states [21].

Figure 12 shows the amplitude A (top) and phase derivative $\partial_t \Phi$ (bottom) versus time for 100 μs of background (noise) data. Please refer to figure 13 and the following paragraph to compare to plasma data. The phase derivative data has been shifted slightly away (up (down) for positive (negative) derivatives, respectively) from zero for clarity. The amplitude does not vary much on the scale shown (same scale as for figure 13), but the phase derivative varies enormously; this is understandable, since it is the derivative of a noisy signal.

In figure 13, we show two plots like the one shown for background data. The left hand plots show 100 μs of dithering L-mode data, the right hand plots show dithering H-mode data. The typical lifetime of an event is a few microseconds, compare to figure 2 in [20]. By visual inspection, the amplitudes are hard to tell apart; but the phase derivatives are distinct: the L-mode derivative seems to have a larger magnitude and to be more 'clean' than the 'grassy' H-mode derivative.

To elucidate the differences observed between the L- and H-mode phase derivatives, we show a plot of the phase derivative averaged over 100 μs, $\langle \partial_t \Phi \rangle$, and a plot of the average of the absolute value of the phase derivative, $\langle |\partial_t \Phi| \rangle$. The two different averages of the phase derivative are shown in the bottom row of figure 14, while the H_α-signal is shown for reference in the top row.

The averages tell us different things: the standard average includes the sign, i.e. direction, of the density fluctuations. If this average is different from zero, fluctuations travelling in one direction dominate over those in the opposite direction. The left hand column of figure 14

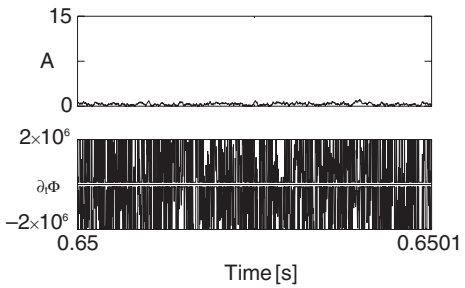

Figure 12. Representation of background data. Top: signal amplitude versus time for 100 μs, bottom: time derivative of the phase for the same interval. The data has been band pass filtered between 50 kHz and 1 MHz.

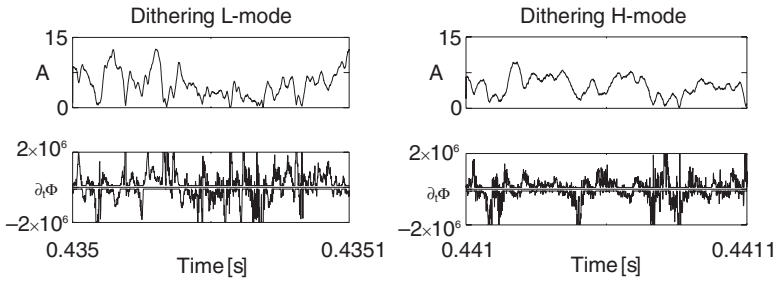

Figure 13. Representation of L-mode (left) and H-mode (right) data during dithering. Top: signal amplitude versus time for 100 μs, bottom: derivative of the phase with respect to time for the same interval. The data has been band pass filtered between 50 kHz and 1 MHz.

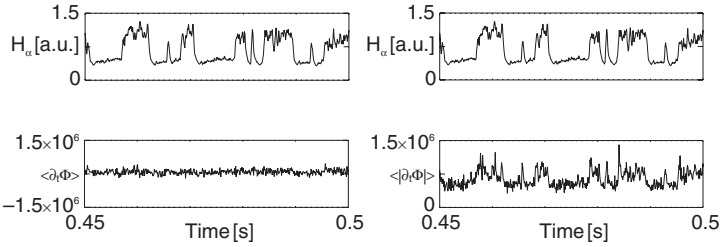

Figure 14. Left: H_α (top) and average of phase derivative (bottom) for 50 ms of a dithering plasma. Right: H_α (top) and average of the absolute value of the phase derivative (bottom) for the same time interval.

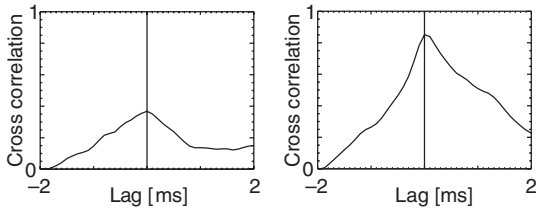

Figure 15. Left: cross correlation between H_α-light and the average phase derivative, right: cross correlation between H_α-light and the average of the absolute value of the phase derivative. The time lag resolution is 100 μs.

shows that this is not the case. The average of the absolute value of the phase derivative contains information on the speed U (size of velocity) of the fluctuations. The direction is here ignored; the right hand column of figure 14 shows that this quantity is correlated with the H_α-light. The average is high in L-mode and low in H-mode, meaning that the speed of fluctuations is faster in L-mode than H-mode. Since $\langle|\partial_t \Phi|\rangle = k_\perp U$, where $k_\perp$ is the measured wavenumber, a $\langle|\partial_t \Phi|\rangle$ value of $7.9 \times 10^5\,\mathrm{s}^{-1}$ (average over all L-mode time windows, see the bottom right hand plot of figure 14) at $14\,\mathrm{cm}^{-1}$ corresponds to a speed U_L of $564\,\mathrm{m\,s}^{-1}$. The H-mode $\langle|\partial_t \Phi|\rangle$ average is $5.2 \times 10^5\,\mathrm{s}^{-1}$, meaning that $U_H = 371\,\mathrm{m\,s}^{-1}$. The speed ratio, U_L/U_H, is therefore about 1.5; our method developed here complements calculating mean frequencies for several wavenumbers (see figure 11 in [5]) but can be made using a single discharge. The L- and H-mode speeds found are close to those found in [5].

To quantify the correlation between the H_α-signal and the different phase derivative signals, we show cross correlations in figure 15. The time lag is in units of 100 μs up to ± 2 ms and positive lags mean that the density fluctuation signal occurs first. Correlating between H_α and the average phase derivative yields a modest maximum correlation at zero time lag of 40%. In contrast, the correlation with the average of the absolute value of the phase derivative is above 80% at zero time lag. Further, the cross correlation function is asymmetric, insofar as it is larger for positive lags compared to negative ones. As noted in connection to figure 9, this is due to the fact that H_α falls off slowly, whereas density fluctuations drop immediately at an L–H transition.

6. Conclusions

We have in this paper treated a single discharge with the purpose of studying whether steady-state L-mode and H*-mode possess the same characteristics as those found by separating dithering phases into L- and H-mode time windows [5].

Based on the analysis in the present paper, it is clear that this indeed is the case. Apart from a couple of quantitative differences (e.g. an additional high frequency feature in H*-mode), subsets of a dithering period and corresponding quiescent phases are identical.

The remaining open question that we have not answered is whether L-mode dithers are collections of closely spaced ELMs or a distinguishable phenomenon. Unfortunately, we do not have sufficient measurements of discharges displaying single ELM activity to answer this question. If we were to speculate, our opinion would be that dithers are indeed collections of overlapping ELMs, where a single ELM has a lifetime of $\sim$100 μs—which is the correlation time we found, both in dithering and steady-state L-mode.

Acknowledgments

Technical assistance by H E Larsen, B O Sass, J C Thorsen (Risø) and M Fusseder, H Scholz, G Zangl (Garching) was essential for the operation of LOTUS. N P B wishes P Garrett, B Hillman, R Hirst, J Moginie and M Rotsey the best of luck in their future endeavours.

References

[1] Hahm T S 2002 *Plasma Phys. Control. Fusion* **44** A87
[2] Gohil P 2002 *Plasma Phys. Control. Fusion* **44** A37
[3] Hirsch M *et al* 2000 *Plasma Phys. Control. Fusion* **42** A231
[4] Zohm H 1994 *Phys. Rev. Lett.* **72** 222
[5] Basse N P *et al* 2002 *Phys. Plasmas* **9** 3035
[6] Basse N P *et al* 2000 *27th EPS Conf. ECA* B **24** 940
[7] Zoletnik S *et al* 2002 *Plasma Phys. Control. Fusion* **44** 1581
[8] Basse N P *et al* 2003 *Nucl. Fusion* **43** 40
[9] Grigull P *et al* 2001 *Plasma Phys. Control. Fusion* **43** A175
[10] Giannone L *et al* 2000 *Plasma Phys. Control. Fusion* **42** 603
[11] Baldzuhn J *et al* 1998 *Plasma Phys. Control. Fusion* **40** 967
[12] Koch R A and Tang W M 1978 *Phys. Fluids* **21** 1236
[13] Lehnert B 1966 *Phys. Fluids* **9** 1367
[14] Biglari H *et al* 1990 *Phys. Fluids B* **2** 1
[15] Saffman M *et al* 2001 *Rev. Sci. Instrum.* **72** 2579
[16] Fonck R J *et al* 1993 *Phys. Rev. Lett.* **70** 3736
[17] Watterson R L *et al* 1985 *Phys. Fluids* **28** 2857
[18] Bendat J S and Piersol A G 2000 *Random Data: Analysis and Measurement Procedures* (New York: Wiley)
[19] Zerbini M *et al* 1999 *Plasma Phys. Control. Fusion* **41** 931
[20] Antar G *et al* 1999 *Plasma Phys. Control. Fusion* **41** 733
[21] Basse N P *et al* 2001 *9th European Fusion Theory Conf. (Elsinore, Denmark)* www.risoe.dk/ ofd/fusion2001.htm